Available online at www.sciencedirect.com
ScienceDirect
Trans. Nonferrous Met. Soc. China 32(2022) 2091−2109
Transactions of Nonferrous Metals Society of China
www.tnmsc.cn

Effects of temperature and time on three-dimensional microstructural evolution of semi-solid 2A14 aluminum alloy during short process preparation of semi-solid billets

Ying-ze LIU[1], Ju-fu JIANG[1], Guan-fei XIAO[1], Ying ZHANG[1], Min-jie HUANG[1], Ying WANG[2]

1. School of Materials Science and Engineering, Harbin Institute of Technology, Harbin 150001, China;
2. School of Mechatronics Engineering, Harbin Institute of Technology, Harbin 150001, China

Received 22 June 2021; accepted 27 December 2021

Abstract: To shorten the preparation process of semi-solid billets, semi-solid billets of 2A14 aluminum alloy were prepared by wrought aluminum directly semi-solid isothermal treatment (WADSSIT) process. Three-dimension (3D) combined microstructure evolution, namely transverse direction (TD) surface, rolling direction (RD) surface, and normal direction (ND) surface, was studied. Effects of temperature and holding time on average grain size and average shape factor were investigated. The results showed that the optimum conditions for preparation of 2A14 semi-solid billets by this process were 615 °C and 20 min (average grain size of 124 μm and shape factor of 0.81). Electron backscatter diffraction (EBSD) observations indicated that the microstructure was completely recrystallized when it was heated to 600 °C. Grain size was increased with the increase of temperature and grew up slowly with the holding time prolonging. Roundness was increased with increase of holding time but was not sensitive to temperature.
Key words: 2A14 aluminum alloy; three-dimensional microstructure; semi-solid billet; microstructure evolution

1 Introduction

2A14 aluminum alloy is a wrought aluminum alloy of Al−Cu series, and its comprehensive mechanical properties are significantly better than those of cast aluminum alloys [1,2]. Because of its high strength, great machining performance, good contact welding and spot welding performance, it is often used to manufacture aircraft die forgings that carry high loads [3−5]. In addition to copper, the alloy also contains alloying elements such as silicon, magnesium, and manganese, which can be heat-treated and strengthened by using solution treatment and artificial or natural aging. The main strengthening phases of the 2xxx series aluminum alloys are Al_2Cu and Al_2CuMg [6].

Semi-solid processing (SSP) is a special near-net-shape technology [7−10]. SAMAT et al [11] reported the mechanical properties of thixoformed Al−Si−Cu alloy automotive connecting rods, and comparison with the gravity-cast parts showed improvement of 95% and 22% in UTS and hardness with the resulting values of 340 MPa and HV 122, respectively. CHEN et al [12] conducted a compound forming method of the 7075 aluminum alloy. The complex zone of semi-solid thixoforming and the simple zone of solid plastic deformation forming were realized by gradient heating. The Vickers hardness was increased from semi-solid forming zone to the transition zone and then to the plastic forming zone in gradient. ABBASIPOUR et al [13] compared the tribological behavior of A356-CNT nanocomposites fabricated by various techniques, and found that the existence of the solid phase in semi-solid process could improve the wear

Corresponding author: Ju-fu JIANG, Tel: +86-18746013176, E-mail: jiangjufu@hit.edu.cn;
Ying WANG, Tel: +86-15945697615, E-mail: wangying1002@hit.edu.cn
DOI: 10.1016/S1003-6326(22)65933-8
1003-6326/© 2022 The Nonferrous Metals Society of China. Published by Elsevier Ltd & Science Press

properties of the nanocomposite samples than fully liquid casting.

SSP requires special steps to prepare suitable semi-solid billets for thixoforging [14−16]. There are many methods for preparing semi-solid billets, such as magnetohydrodynamic stirring (MHD) [17], cooling slope casting [18], strain induced melt activated (SIMA) [19], and recrystallization and partial melting (RAP) [20,21]. CAMPO et al [22] investigated the globular microstructure formation and coarsening of semi-solid Ti−Cu alloys fabricated by RAP method, and concluded that refined globular microstructure was attributed to the break-up mechanism of the applied hot forging process prior to heating to the semi-solid state. CZERWINSKI [23] gave a detailed review of the specific classification of SSP, various methods and differences for preparation of semi-solid billets. In addition, severe plastic deformation (SPD) processes have been used for pre-deformation to prepare semi-solid billets, for example, equal channel angular extrusion (ECAE) [24,25], equal channel angular pressing (ECAP) [26], repetitive upsetting-extrusion (RUE) [27], cyclic upsetting-extrusion (CUE) [28], rotary swaging (RS) [29], and accumulative back extrusion (ABE) [30]. These methods are similar in principle, increasing the deformation energy storage to facilitate recrystallization and remelting of the semi-solid billets.

Despite the advantages of SSP in resource conservation, green manufacturing and sustainable production, the fabrication of wrought aluminum alloy parts is still dominated by forging due to the complexity of the SSP. Hence, the study of short process SSP forming technology is necessary. The preparation of semi-solid billets is the most important part of the SSP. Commonly, SIMA and RAP methods are used for fabricating semi-solid billets, both of which are complex processes [12,31,32]. Therefore, it is valuable to shorten the preparation process of semi-solid billets. A short process called wrought aluminum directly semi-solid isothermal treatment (WADSSIT) was proposed by heating the mass-supplied hot-deformed wrought alloys directly to fabricate semi-solid billets [33,34]. Excellent formability and good mechanical properties of formed parts can be achieved by these billets. However, the microstructure evolution of 2A14 aluminum alloy during the semi-solid isothermal treatment of the WADSSIT has not yet been investigated.

In this work, semi-solid billets of 2A14 alloy were prepared by a novel short process called WADSSIT method. This method has important guiding significance for shortening the semi-solid billet preparation process and reducing the semi-solid billet cost. The size and morphology of the solid particles in the semi-solid billet and the distribution of solid and liquid phases play an important role in the properties of the semi-solid billet. In the semi-solid billet of wrought aluminum 2A14, the solid phase is an Al-based solid solution, and the liquid phase is a multi-element eutectic component with a low melting point. The effects of the holding temperature and holding time on the microstructure evolution were studied from the three-dimensional direction. The kinetic analyses of the coarsening process were carried out via the Lifshitz and Slyozov and Wagner (LSW) coarsening kinetics [35,36] model.

2 Experimental

The material used in this work is a 2A14 aluminum alloy hot-rolled plate purchased from Northeast Light Alloy Co., Ltd., China. The original ingot thickness is 500 mm, and the final rolled thickness is 50 mm, so the cumulative deformation ratio is 90%. With an Axios PW4400 X-ray fluorescence spectrometer (XRF) equipment, the chemical composition of the aluminum alloy is shown in Table 1. The main alloying element in the alloy is copper, with a content of 4.37 wt.%, which is lower than the maximum copper content that can be dissolved in solid high-temperature aluminum (5.65 wt.%). Due to deviating from the copper content of the aluminum and copper binary eutectic alloy, the solid−liquid temperature range is very wide, but the casting performance is poor. As shown in Fig. 1, a differential scanning calorimetry (DSC) curve was obtained via a STA449F3 differential scanning calorimeter. The semi-solid temperature range of the aluminum alloy is between 512 and 663 °C, and there is a pre-melted eutectic absorption peak between 512 and 530 °C. The heating rate during the test is 10 °C/min. To determine the fraction of solid (f_s), it is assumed that the solid and the liquid phases have the same heat capacity (c_p), the latent heat of fusion (L) is

Table 1 Chemical composition of 2A14 aluminum alloy (wt.%)

Alloy	Cu	Si	Mn	Mg	Fe	Ti	Zn	Ni	Al
Standard	3.9−4.8	0.6−1.2	0.4−1.0	0.4−0.8	≤0.7	≤0.15	≤0.3	≤0.1	Bal.
Sample	4.3700	0.9164	0.7811	0.5893	0.1765	0.0249	0.0274	0.0064	Bal.

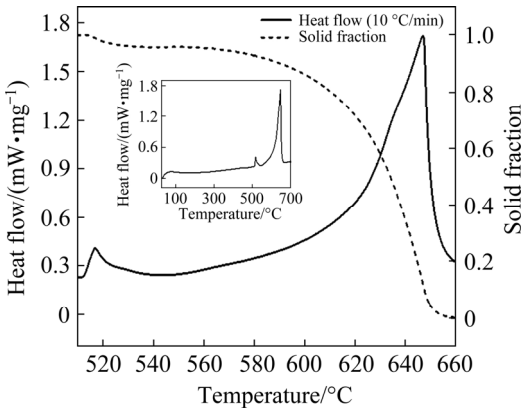

Fig. 1 DSC curve and solid fraction versus temperature of 2A14 Al alloy

constant. Derived from the enthalpy of fusion equation $H=c_pT+f_lL$, f_s can be determined by

$$f_s(T)=1-\left[\frac{(H-H_{\text{solidus}})-c_p(T-T_{\text{solidus}})}{(H_{\text{liquidus}}-H_{\text{solidus}})-c_p(T_{\text{liquidus}}-T_{\text{solidus}})}\right] \tag{1}$$

where H is the enthalpy, f_l is the fraction of liquid, and T is the temperature. We integrated the DSC results and obtained the theoretically calculated solid fraction vs temperature curve of the alloy, as shown in Fig. 1. Although the solid fraction of the alloy is not only related to temperature, but also affected by the residence time at that temperature, it is most affected by temperature, so it still has a strong reference value [37].

A muffle furnace was used for semi-solid isothermal treatment. Dozens of rectangular parallelepipeds with dimensions of 8 mm × 10 mm × 12 mm were cut from the hot-rolled plate. The three-dimensional dimensions were all different in order to distinguish the relative direction of the rectangular parallelepiped on the rolled plate. The temperature of the muffle furnace was heated to the target temperature and kept for more than 30 min to make the temperature in the furnace uniform. The samples were then placed in a muffle furnace for heating. A high-temperature sensitive thermocouple was placed at the bottom of the sample to monitor the temperature of the sample in real time. The heating environment is an air atmosphere and no protective atmosphere is needed to control oxidation. Because of the characteristics of aluminum alloy, heating can form a dense oxide film on the surface to prevent further oxidation inside. In the subsequent characterization, the oxide film on the surface was removed using sandpaper. For a sample of this size, it took 5 min to heat to the target temperature. It should be noted that the holding time does not include the heating time. Seven temperatures were set as 580, 590, 595, 600, 610, 615 and 620 °C, and six holding time was set as 5, 10, 15, 20, 25, and 30 min. There were a total of 42 (6 × 7) experimental conditions.

The samples were quenched into cold water immediately when the holding time reached the target time to retain their microstructure morphology. Then the samples were ground using 200, 400, 600, 1200, 1500 and 2000 grit sandpapers in turn. After that, the samples were polished on a real velvet polishing disc sprayed with 1 μm diamond micro-powder at 1200 r/min for 5 min. And then the samples were etched by chemical etching. The chemical solution for etching was Keller reagent with a solution formulation (2.5% HNO_3 + 1.5% HCl + 1% HF + 95% H_2O). The etching time was 25 s. The microstructure of the samples was observed by using a GX71 optical microscope (OM) and a SUPRA55 scanning electron microscope (SEM). Each sample was processed on three different directions of surfaces according to the above steps to characterize the microstructure changes in the three-dimensional direction. The three-dimensional microstructure in this work shows the combined structure of the three main directions, namely TD, RD and ND surfaces. The image pro plus (IPP) software was used to calculate the size and roundness of the solid particles. The average diameter (D_{eq}) and shape factor (F_{eq}) are defined by Eqs. (2) and (3), respectively.

$$D_{\text{eq}}=\sum_{i=1}^{N}\sqrt{\frac{4A_i}{\pi}}/N \tag{2}$$

$$F_{eq}=\sum_{i=1}^{N}\frac{4\pi A_i}{P_i^2}/N \quad (3)$$

where N is the total number of the solid grains, A_i is the area of the grain i, and P_i is the perimeter of the grain i.

3 Results and discussion

3.1 Microstructural evolution in semi-solid state

Figure 2 shows the recrystallization process during continuous heating. The temperature change of the sample in the muffle furnace with time was monitored by a high-temperature sensitive thermocouple in real time. The three colors of red, yellow and blue represent deformed grain structure, sub-grain structure and recrystallized grain structure, respectively. This was obtained by calculating the grain orientation spread (GOS) index of every grain in the electron backscatter diffraction (EBSD) results. The GOS value of grain can reflect recrystallization because there is a mean orientation in grain, and GOS of the grain is the average value of the misorientation between all pixels in the grain and the mean orientation [38]. The average misorientation between each pixel point relative to the grain mean orientation in the deformed grain is relatively large, while the GOS in the recrystallized grain is relatively small. There is no strict definition of the GOS value among the three grain structures, and different metals will also produce different definition standards. According to the commonly used values of aluminum alloy, in this work, the GOS value below 1.8° was regarded as the recrystallized grain structure, that between 1.8° and 3° was regarded as the sub-grain structure, and that greater than 3° was regarded as the deformed grain structure [39,40].

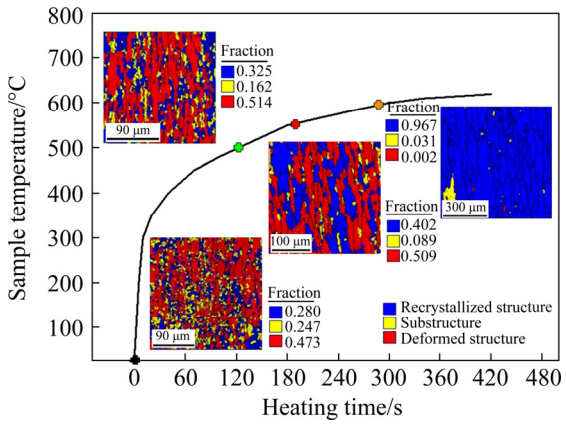

Fig. 2 Evolution of recrystallization during continuous heating of hot-rolled 2A14 aluminum alloy

The hot-rolled microstructure Fig. 2 had a dynamic recrystallized (DRX) structure, so there were some recrystallized structures and sub-structures. When the temperature was continuously increased to 505 °C, the corresponding heating time was only 2 min, some crystal grains merged and grew up. The relative proportions of the three structures changed little. When the sample was heated to 555 °C, the corresponding heating time was 3 min. The proportion of recrystallized structure was slightly increased, indicating that recrystallization starting temperature was 555 °C. When the specimen was heated to 580 °C, the corresponding heating time was 5 min, the grain size grew up further, and the proportion of recrystallized structure increased to 0.967. It shows that the termination temperature of recrystallization was 580 °C. The results show that the hot-rolled 2A14 aluminum alloy underwent complete recrystallization after the continuous heating process, and the size of the grains begun to grow.

Figure 3 shows the evolution of the three-dimensional microstructures of 2A14 aluminum alloy held at 580 °C for 5−30 min. The corresponding liquid fraction was 0.07. The isothermal time was measured after the sample was heated to the target temperature. The black area in the figure was the liquid phase in the semi-solid structure. It can be seen that the semi-solid structure included two parts: solid phase and liquid phase. The solid phase was an aluminum-based solid solution, while the liquid phase was a low melting point copper-rich eutectic structure. In the semi-solid structure, the liquid phase existed in three forms: liquid film (LF), liquid droplets (LD) inside the solid grain, and grain boundary liquid (GBL) [34].

At 580 °C, the fraction of the liquid phase was low, and the liquid phase was mainly composed of LF and LD inside the solid grain, and the thickness of the LF was very thin. With the extension of holding time, the size of the solid phase grains was gradually increased. On the normal direction (ND) surface, the size of the solid phase particles was very uniform, and the shape was almost circular. On the transverse direction (TD) surface, the size of the solid phase particles was not uniform, and all were elliptical. On the rolling direction (RD) surface, the

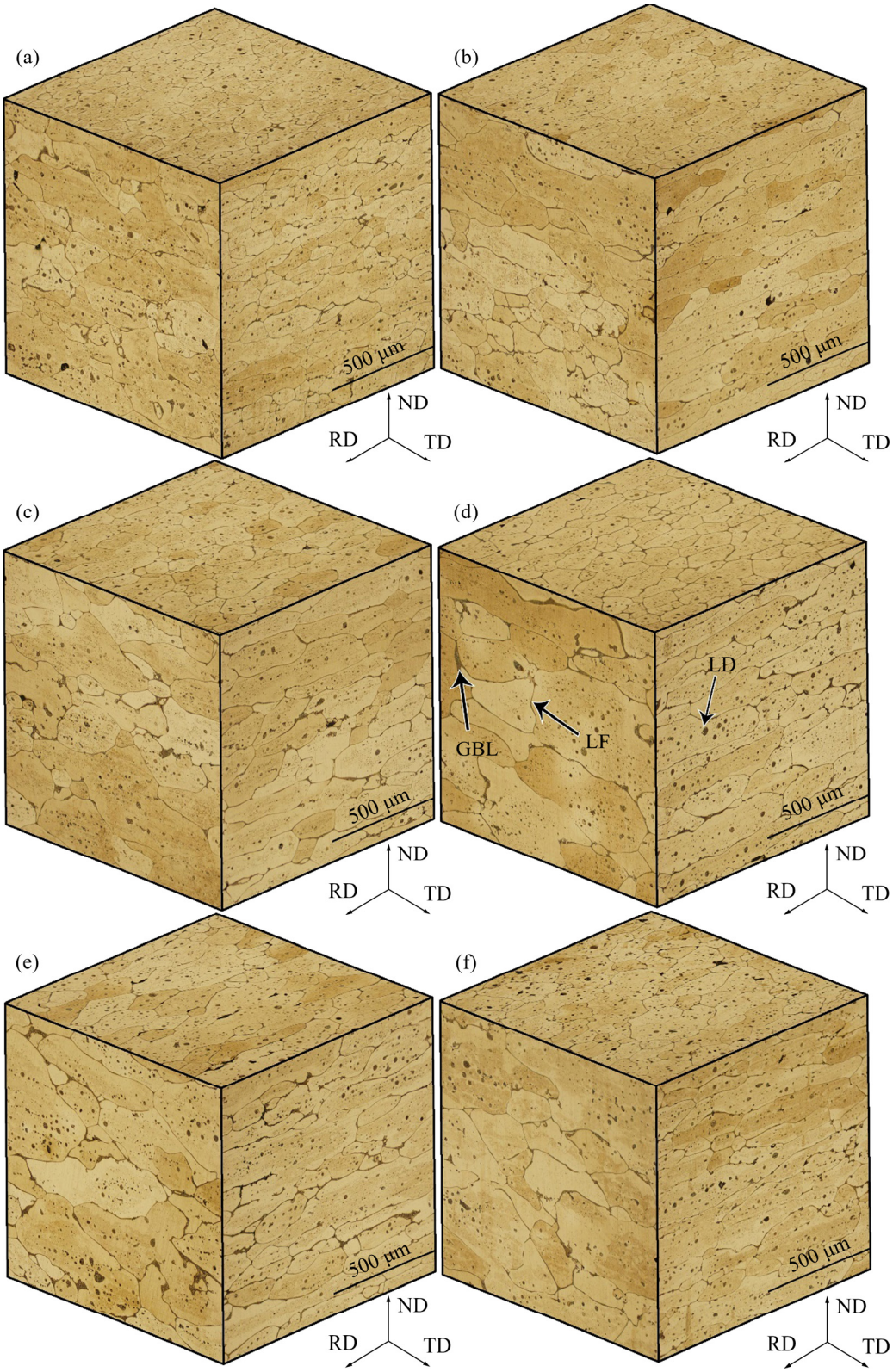

Fig. 3 3D microstructures of 2A14 samples treated at 580 °C for various time: (a) 5 min; (b) 10 min; (c) 15 min; (d) 20 min; (e) 25 min; (f) 30 min

size of the crystal grains was extremely uneven and the shape was irregular, and huge polygonal crystal grains appeared in the heat preservation for 15 min. The distribution of droplets inside the grain was relatively uniform, and there was no convergence phenomenon as the holding time increased.

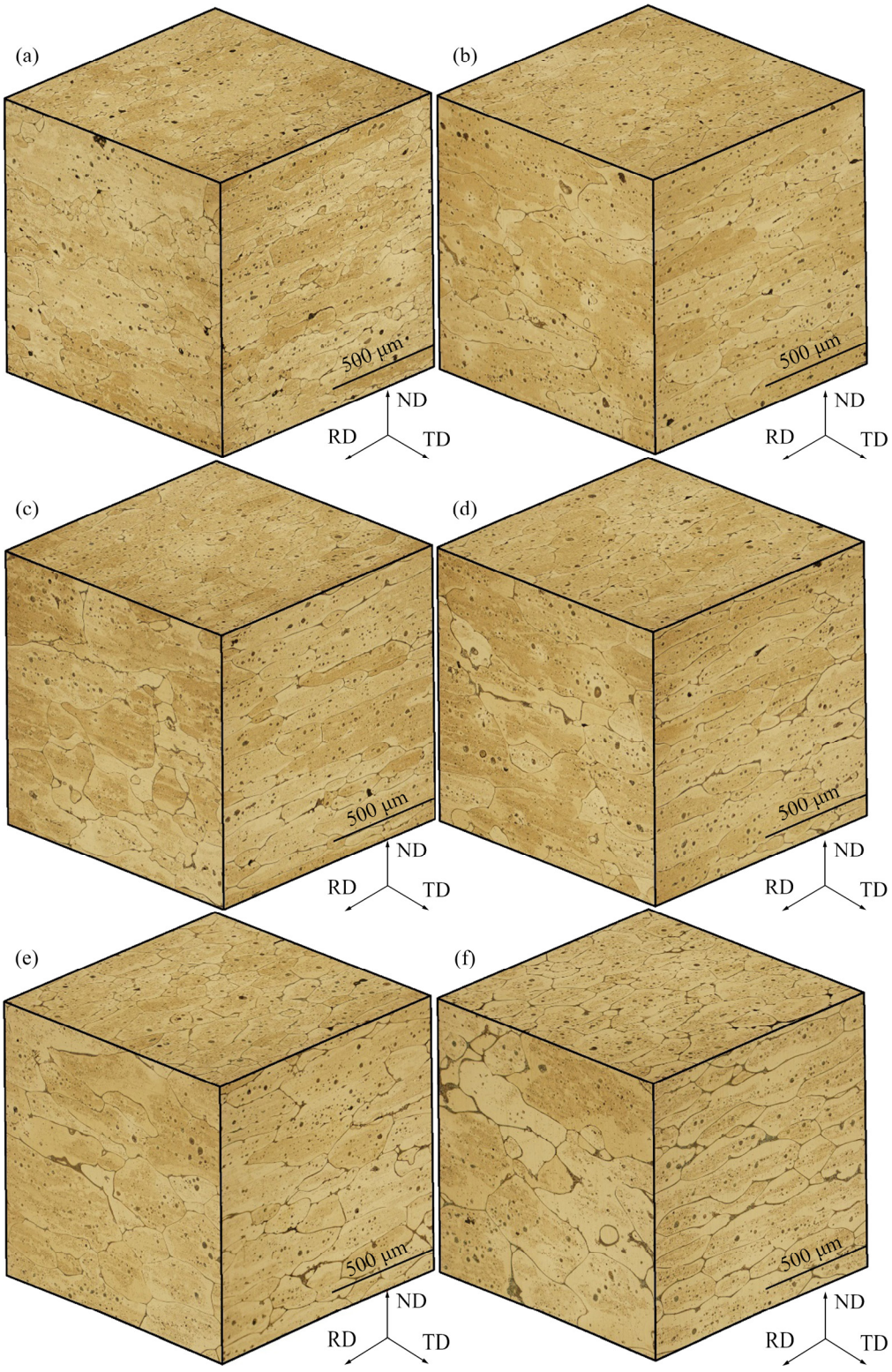

Fig. 4 3D microstructures of 2A14 samples treated at 590 °C for various time: (a) 5 min; (b) 10 min; (c) 15 min; (d) 20 min; (e) 25 min; (f) 30 min

Figure 4 shows the evolution of the 3D microstructures of 2A14 aluminum alloy held at 590 °C for 5−30 min. The corresponding liquid fraction is 0.10. At 5 min and 10 min, the size of the solid particles was slightly smaller than that at the corresponding time at 580 °C. The LF at 590 °C was slightly thicker than that at 580 °C. At 590 °C, the change tendency of solid phase particle size and

the distribution of solid phase particle shape were consistent with those at 580 °C.

The size of the solid phase particles was affected by many factors. WANG et al [41] concluded that initial grain size was related to the pre-deformation process and the subsequent recrystallization. Besides, grain size is increased with isothermal holding time and temperature. Coarsening of grain is mainly attributed to coalescence and Ostwald ripening, with increasing isothermal holding time and temperature, the latter plays an increasingly important role. When the temperature was low, the main aspects were recrystallization and coarsening of solid particles. Increasing the temperature would promote the occurrence of recrystallization but at the same time would also accelerate the coarsening of the solid phase particles. The effect of increasing temperature on the acceleration of solid-phase particle coarsening existed in the entire semi-solid isothermal treatment process. However, the promoting effect of increased temperature on recrystallization only occurred in the recrystallization process.

Factors that promote recrystallization include increasing the temperature (raising the liquid phase fraction), increasing the deformation of the alloy, and extending the holding time. LI et al [24] studied the recrystallization process of Mg alloy after ECAP and found that the second phase particles (*I* phase) hinder recrystallization. ATKINSON et al [42] reported the pinning effect of the dispersoid particles present in the 7075 aluminum alloy, which were resistant to the recrystallization of the alloy. Extending holding time can make the liquid phase dissolve the second phase particles, thus promoting recrystallization.

The thickness of the LF was also determined by many factors, mainly including the liquid phase fraction and the size of the solid phase particles. Calculation by TZIMAS and ZAVALIANGOS [43] showed that assuming liquid uniformly surrounding the solid grain, the average liquid film thickness was 1.8 μm with a spherical grain size of 50 μm at f_l=0.2, and the increase of solid-phase grain size thinned the liquid film. An increase in the liquid phase ratio would thicken the liquid film. The increase in the size of the solid particles would reduce the total surface area of the liquid film per unit volume and increase the thickness of the liquid film.

Figure 5 shows the evolution of the three-dimensional microstructures of 2A14 aluminum alloy held at 595 °C for 5−30 min. The corresponding liquid fraction is 0.12. The microstructure at 595 °C exhibited a thinner thickness of LF compared to 580 and 590 °C. This is because although the temperature increased, the fraction of the liquid phase changed very little (0.10 at 590 °C while 0.12 at 595 °C). And the increase in temperature promoted the recrystallization during the heating process, making the size of the solid phase particles smaller. As a result, the surface area of the liquid film per unit volume increased and the thickness of the liquid film became smaller. However, with the extension of the holding time, the solid phase particles grew faster at 595 °C, so that the final solid phase particle size was close at 580 and 590 °C when the temperature was held for long time.

At the three temperatures of 580, 590, and 595 °C, the fractions of the liquid phase were very similar (0.07 at 580 °C, 0.10 at 590 °C, and 0.12 at 595 °C), the influence of the liquid phase could be ignored, and the difference in microstructure evolution was considered to be caused only by temperature changing. Deformation energy storage and external heat input are the driving forces for recrystallization [44]. The hot-rolled plate consumed a lot of deformation energy in the process of hot rolling. Compared with cold deformation and warm deformation, the deformation energy storage of hot-rolled plates is lower, and higher energy input is required for recrystallization. The increase in temperature could promote recrystallization in the recrystallization stage, but at the same time, the high temperature would aggravate the coarsening of solid particles [42,45]. For this hot-rolled plate, in the process of the WADSSIT, semi-solid billets with equiaxed solid particles in three dimensions cannot be obtained at 580, 590 and 595 °C.

If considering the need to control the size and roundness of the solid particles in the semi-solid billet, it is more conducive to theoretically speed up the heating rate during the heating stage, increase the temperature of the sample during the recrystallization process, but reduce the temperature of the sample during the heat preservation process to obtain a semi-solid billet with fine solid particles and a high roundness.

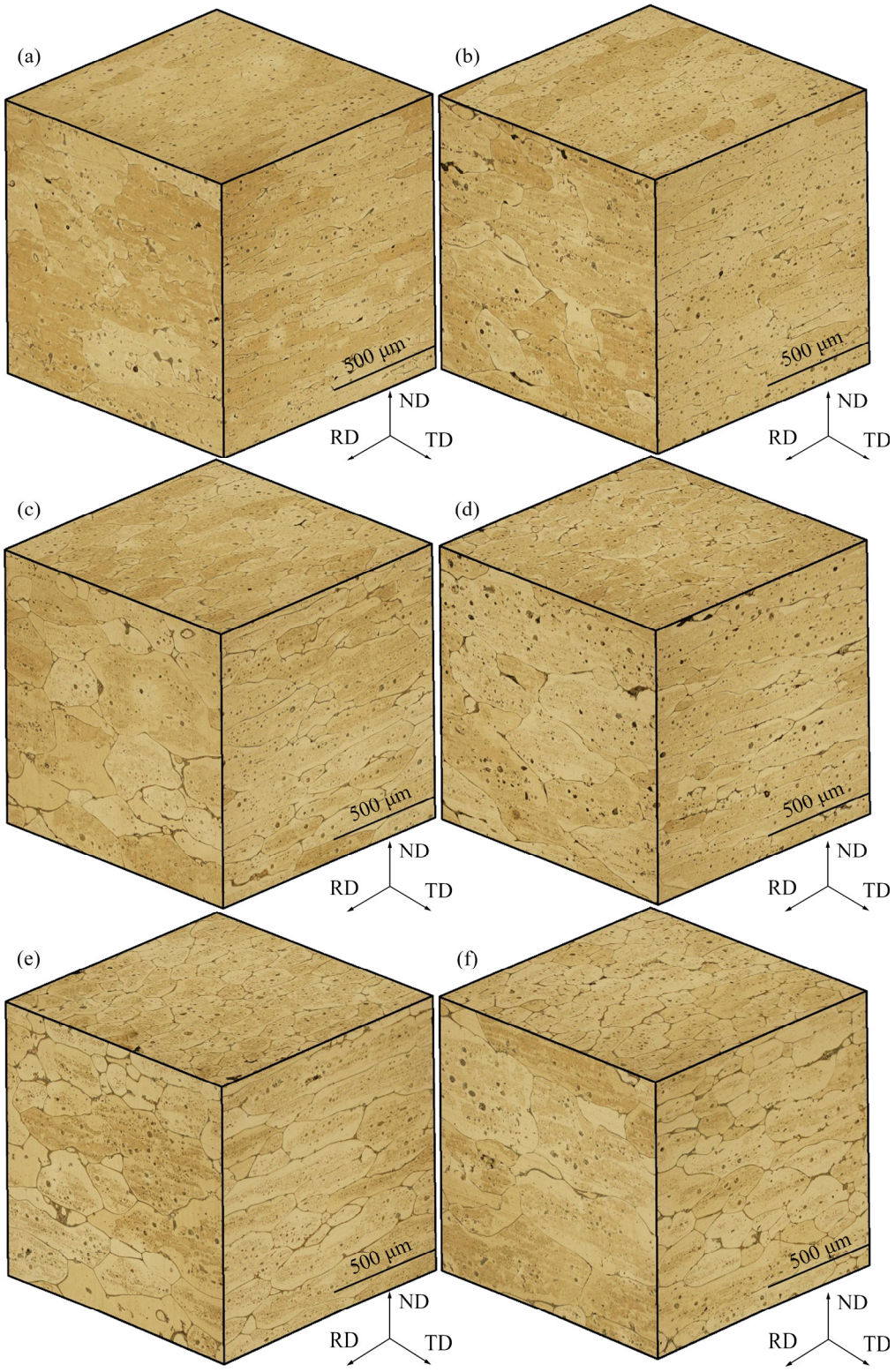

Fig. 5 3D microstructures of 2A14 samples treated at 595 °C for various time: (a) 5 min; (b) 10 min; (c) 15 min; (d) 20 min; (e) 25 min; (f) 30 min

Figure 6 shows the evolution of the 3D microstructures of 2A14 aluminum alloy held at 600 °C for 5−30 min. With the further increase of the holding temperature, the alloy absorbed heat significantly on the DSC curve near 600 °C, indicating that the alloy melted significantly at this temperature and the liquid phase fraction increased significantly. The LF was obviously thick, the LD

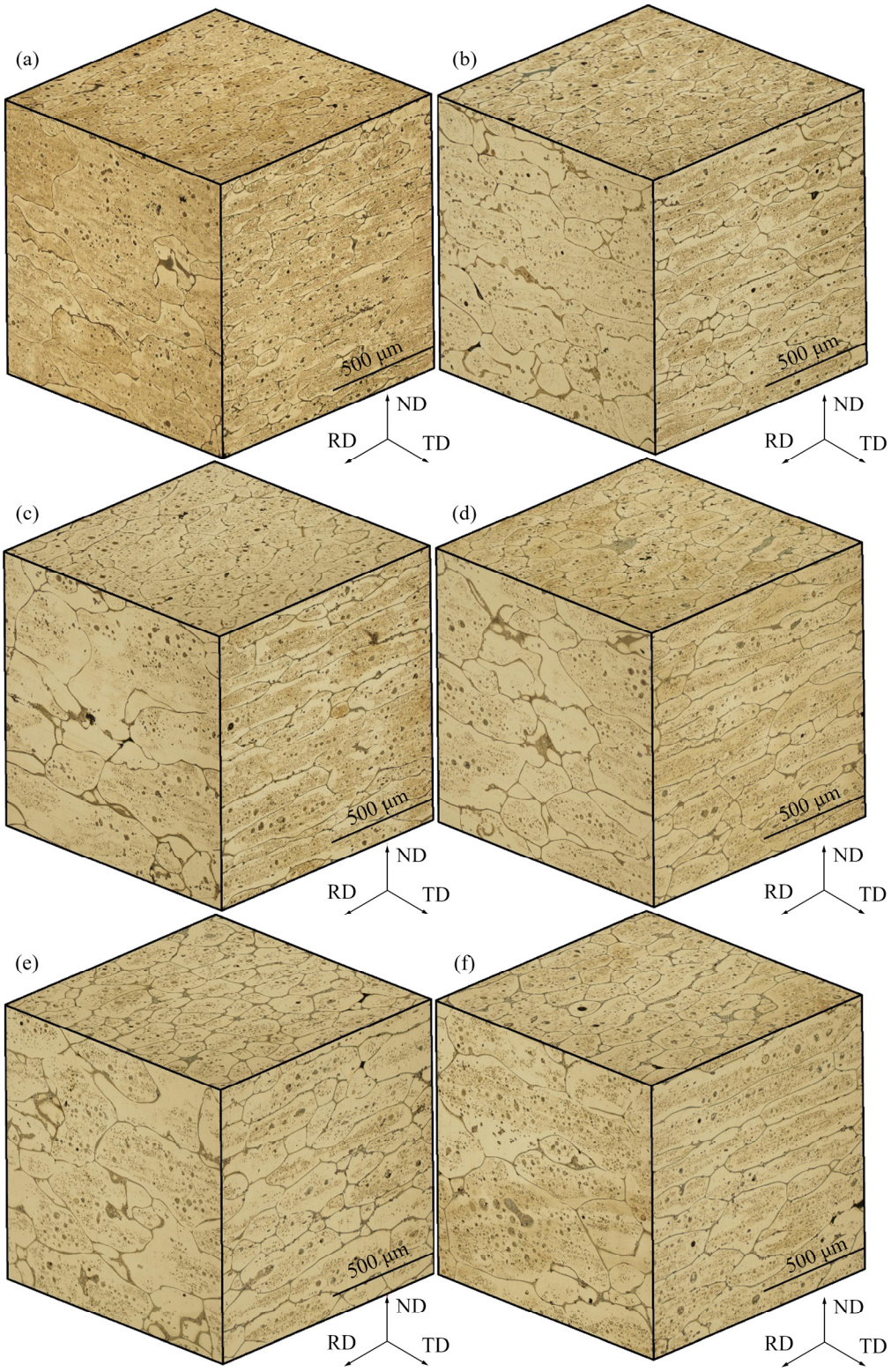

Fig. 6 3D microstructures of 2A14 samples treated at 600 °C for various time: (a) 5 min; (b) 10 min; (c) 15 min; (d) 20 min; (e) 25 min; (f) 30 min

inside the grains increased, and the GBL began to appear. On the ND surface, the solid phase particles were nearly round. On the TD surface, the solid phase particles were still elongated grains, but compared with low temperatures (580, 590 and 595 °C), the roundness of the solid grains was improved. On the RD surface, the size of the solid grains was uneven and the shape was irregular.

Recrystallization is a process of nucleation and growth. The pinning effect of the insoluble matter at the grain boundary is major resistance to recrystallization [42,46]. As the temperature rises, these insoluble substances either dissolve or lose the pinning effect due to further melting of the grain boundaries. This makes the degree of recrystallization at 600 °C higher than that at low temperatures (580, 590 and 595 °C) [41].

Figure 7 shows the evolution of the three-dimensional microstructures of 2A14 aluminum alloy held at 610 °C for 5−30 min. At this time, the

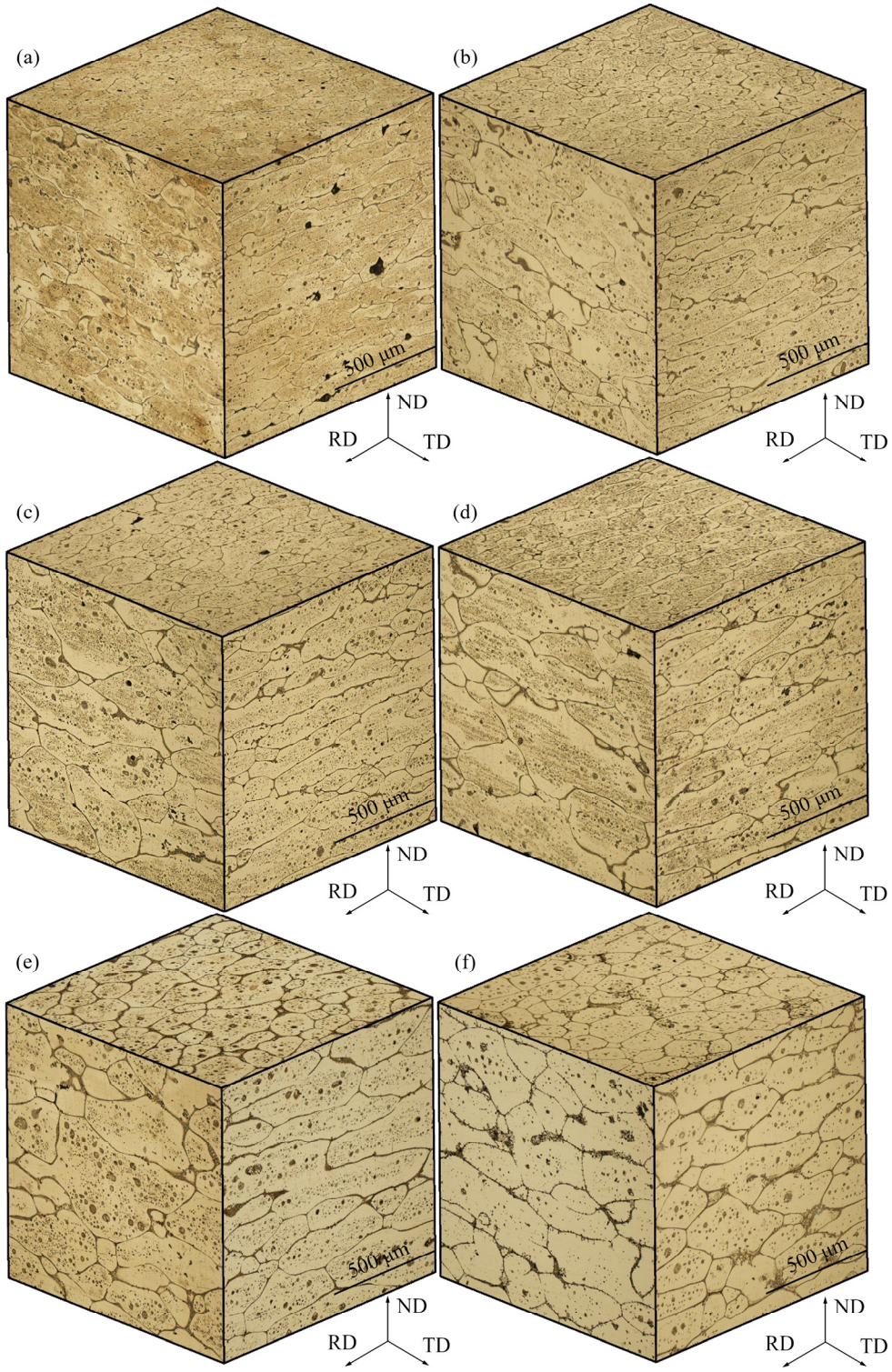

Fig. 7 3D microstructures of 2A14 samples treated at 610 °C for various time: (a) 5 min; (b) 10 min; (c) 15 min; (d) 20 min; (e) 25 min; (f) 30 min

corresponding liquid fraction is 0.2. With the extension of the holding time, the solid phase particles gradually grow up, the edges of the solid phase particles gradually become rounded under the infiltration of the GBL, the GBL becomes more, and the LDs merge into big ones. There is a phenomenon that the GBL is connected to the LD inside the grain. The coarsening mechanism of solid particles includes coalescence mechanism and Ostwald ripening mechanism. Coalescence is the merging of solid particles with close orientations. Ostwald ripening is the melting of small grains and the growth of large grains.

Regardless of the growth mechanism, the driving force for the coarsening of solid particles is the reduction of interfacial energy. When the liquid phase fraction is low, the coarsening mechanism is dominated by coalescence mechanism, and when the liquid phase fraction is high, the coarsening mechanism is dominated by Ostwald ripening [21]. TZIMAS and ZAVALIANGOS [43] considered the effects of coalescence in microstructure evolution of the SIMA process and concluded that the frequency of coalescence is related to the number of adjacent grains since coalescence is closely related to the migration of grain boundaries. GHAZANLOU et al [39] reported the texture evolution of rolled 7075 aluminum, the grain orientation of the hot-rolled aluminum alloy is similar on the ND and TD surfaces, and the close-packed direction tends to be in the RD direction, while the grain orientation on the RD surface is random. So the coalescence on the ND and TD surfaces produced a more uniform organization, while some small grains cannot merge with the surrounding grains because of the large orientation difference on the RD surface.

Figure 8 shows the evolution of the three-dimensional microstructures of 2A14 aluminum alloy held at 615 °C for 5−30 min. The corresponding liquid fraction is 0.25. On the TD surface, the solid grains transform from elongated to near-equiaxed grains. But on the RD surface, the size and shape of the solid particles are still extremely irregular. And the large solid-phase particles wrap the small solid-phase particles. After holding for 5 min (Fig. 8(a)), a large number of small equiaxed solid-phase particles can be seen. When holding at low temperatures (580−610 °C), even if the holding time is only 5 min, the solid grains on the RD surface are already solid phase particles with uneven and irregular sizes (Figs. 3−7(a)). This shows that increasing the temperature is beneficial to promoting the recrystallization of the hot-rolled structure with insufficient deformation storage energy.

Coarsening mechanism of solid particles on the RD surface was dominated by the coalescence mechanism. Because the grain orientations on the RD surface were relatively close during the hot rolling process, the grains were easy to merge and grow. However, the large solid-phase particles wrapped the smaller grains, as marked with circles shown in Fig. 8, indicating that there were a few smaller grains whose orientation was quite different from that of the large solid-phase particles and the grains cannot merge. And in the subsequent isothermal process within 30 min, the small crystal grains will not merge by the large crystal grains. Only after the alloy was further melted, the Ostwald ripening mechanism (small grains melt and large grains grow) would be further developed, resulting in extremely uneven solid particle size on the RD surface.

Figure 9 shows the evolution of the three-dimensional microstructures of 2A14 aluminum alloy held at 620 °C for 5−30 min. The corresponding liquid fraction is 0.30. On the RD surface, the evolution of the microstructure is consistent with that at 615 °C. When the holding time is 5 min (Fig. 9(a)), the solid particles are uniform and fine-equiaxed. In the subsequent heat preservation process, the crystal grains rapidly coarsen and grow. It is speculated that the growth mechanism is the coalescence mechanism. With the extension of the holding time, the liquid phase increases. When the holding time is 30 min (Fig. 9(f)), the secondary dendritic structure can be seen in the structure under water quenching.

3.2 Element distribution of 2A14 aluminum alloy in semi-solid state

Figure 10 shows the microstructure scanning electron microscope-structure backscatter electron (SEM-BSE) images of 2A14 aluminum alloy after isothermal treatment at 615 °C for 20 min under different magnifications. Under the BSE image, the contrast shows the difference in atomic number. As shown in Fig. 10(a), in the semi-solid structure, there is an obvious contrast difference between the

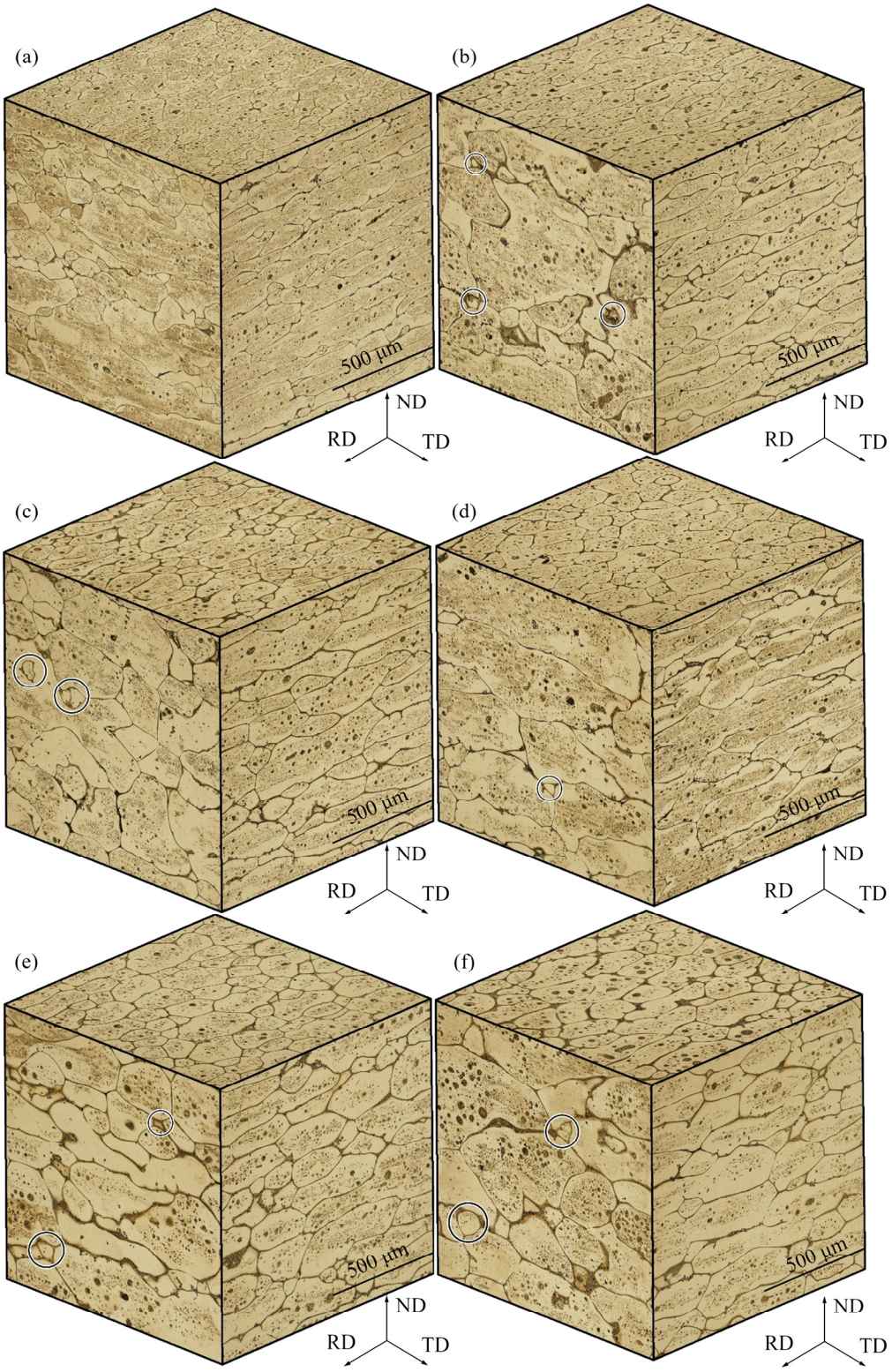

Fig. 8 3D microstructures of 2A14 samples treated at 615 °C for various time: (a) 5 min; (b) 10 min; (c) 15 min; (d) 20 min; (e) 25 min; (f) 30 min

solid phase and the liquid phase. This shows that there is a significant difference in composition between the solid phase and liquid phase. Figure 10(c) shows the image of LD at 5000 times magnification. The liquid phase solidifies when cooled to room temperature to obtain a eutectic structure in which two phases coexist in a lamellar structure. The three points *A*, *B*, and *C* in Fig. 10(b)

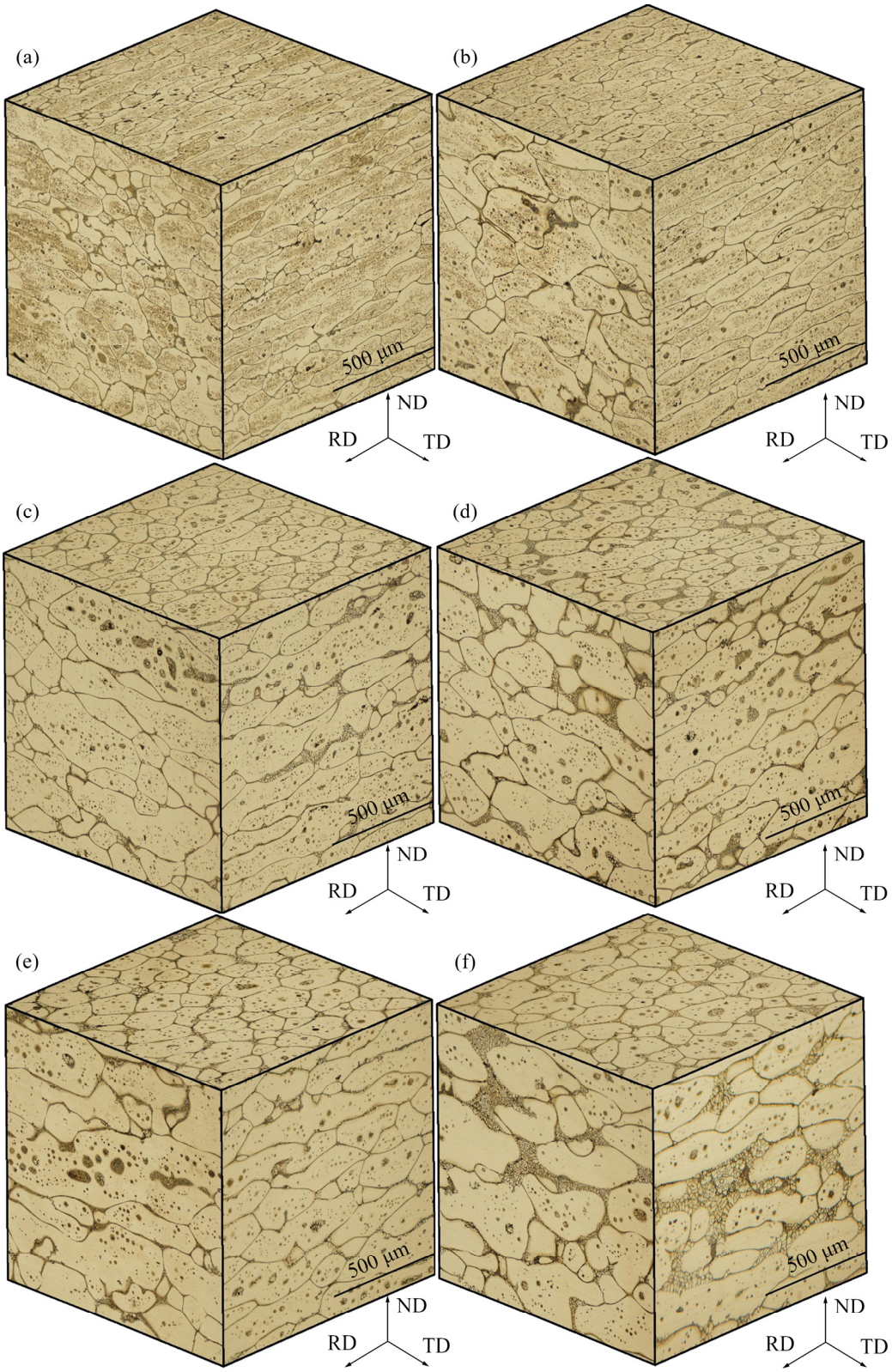

Fig. 9 3D microstructure of 2A14 samples treated at 620 °C for various time: (a) 5 min; (b) 10 min; (c) 15 min; (d) 20 min; (e) 25 min; (f) 30 min

respectively represent the inside of the solid phase particle, the droplet inside the solid phase particle, and the liquid phase at the grain boundary. The point energy spectrum analysis is performed on these three points respectively, and the chemical composition of the three points is shown in Table 2.

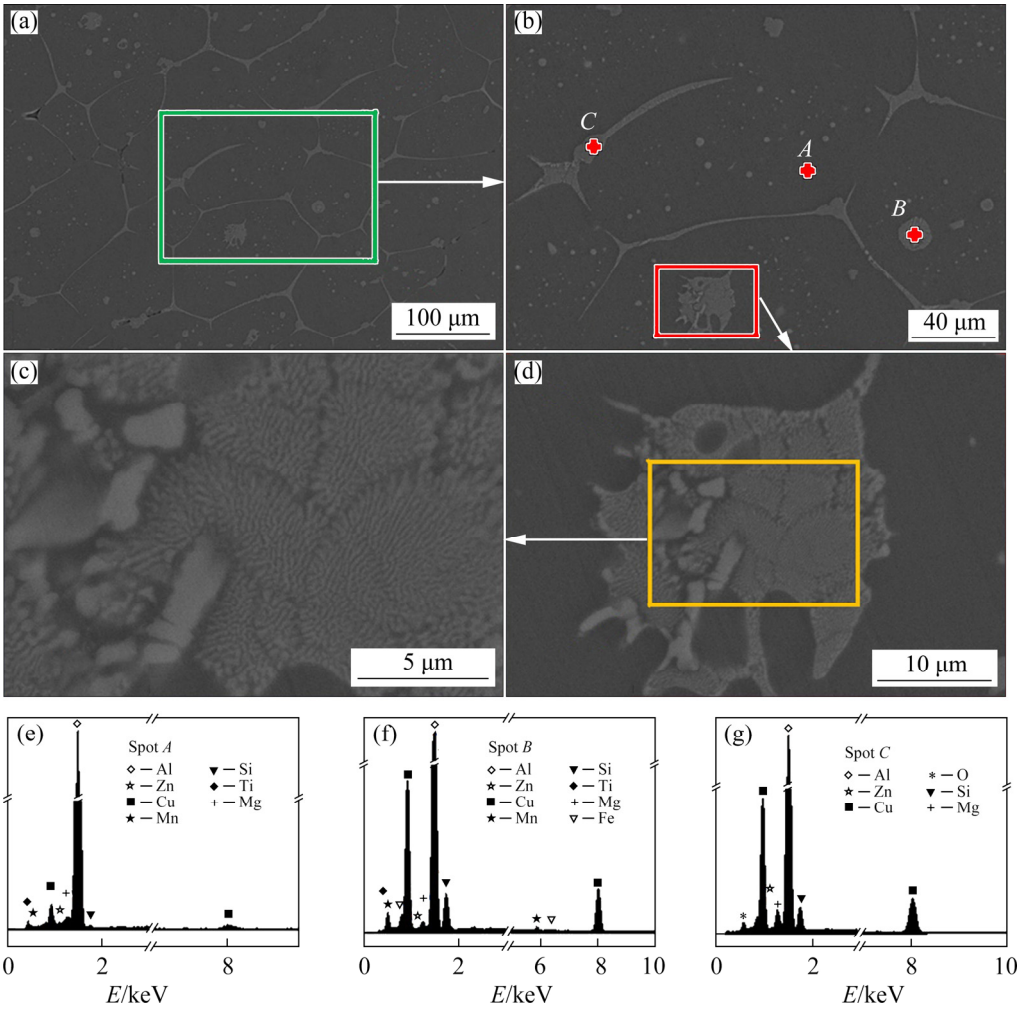

Fig. 10 SEM images of 2A14 aluminum alloy treated at 615 °C for 20 min with different magnifications (a−d), and EDS results of spot *A* (e), spot *B* (f) and spot *C* (g)

Table 2 Chemical compositions of spots corresponding to EDS results in Fig. 10(b) (wt.%)

Spot	Al	Cu	Si	Mn	Mg	Fe	Ti	Zn	O
A	95.73	2.51	0.72	0.03	0.22	−	0.31	0.48	−
B	53.22	35.81	5.60	1.21	3.58	0.46	0.11	−	−
C	53.81	35.72	4.22	−	2.91	−	−	0.50	2.83

It should be noted that the point of the SEM point energy spectrum is not strictly a mathematically infinitely small point, but a volume sphere with a radius of about 2 μm. Therefore, the chemical composition in Table 2 is the statistical composition of a sphere with a radius of about 2 μm at the corresponding point. The internal chemical composition of the solid particles is that a very small amount of various elements are dissolved in aluminum. In the liquid phase, the composition of the liquid droplets is similar to that of the liquid phase at the grain boundary, and they are both low-melting copper-rich eutectic components.

Figure 11 shows the XRD result of 2A14 alloy. The dominant phase in the 2A14 alloy is the α(Al) matrix phase, followed by the θ-Al_2Cu phase. Other alloying elements are solidly soluble in the aluminum matrix phase, and no other phases are evident in the composition of the 2A14 aluminum alloy. Combined with the SEM results in Fig. 10, the solid phase is mainly α(Al) matrix with a variety of dissolved alloying elements, while the liquid phase is mainly a molten θ-Al_2Cu phase with a low melting point.

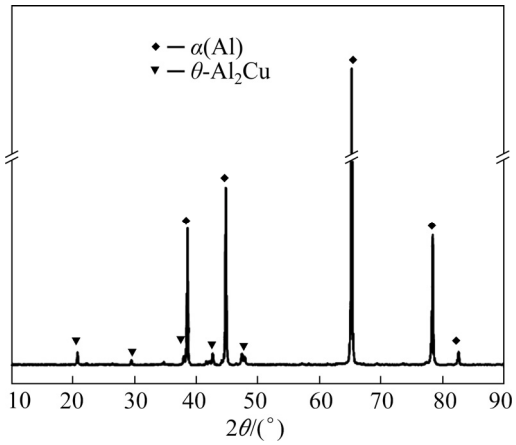

Fig. 11 XRD pattern of distribution of phases in 2A14 aluminum alloy

3.3 Quantitative calculation and coarsening kinetic analysis based on ND surface grain parameters

In order to quantitatively analyze the size and shape factor of the solid particles in the semi-solid billet, the ND surface is selected to calculate the average particle size and roundness of the solid particles. The ND surface is chosen because its crystal grain size and shape are relatively uniform, and it is not easy to cause large errors due to manual selection. Although choosing the ND surface to calculate the size and roundness of the solid phase particles cannot represent the quality of the semi-solid billet, it can reflect the overall change of the solid phase particles with the holding temperature and time.

Figure 12 shows the average size and shape factor of solid particles on the ND surface as a function of temperature and time. The average size of the solid particles increases with the increase of the semi-solid isothermal temperature. The average size of solid particles increases first (5−15 min) and then stabilizes (20−30 min) with the extension of isothermal time. The shape factor of solid particles increases with the increase of isothermal temperature, but it is not obvious. The shape factor of solid particles increases rapidly first with the extension of the isothermal time (5−15 min), and then slowly increases with the extension of the holding time (20−30 min). This is different from the previous experimental results.

Generally, when aluminum alloy is isothermal at the semi-solid temperature, the solid phase grain coarsening phenomenon is very significant with

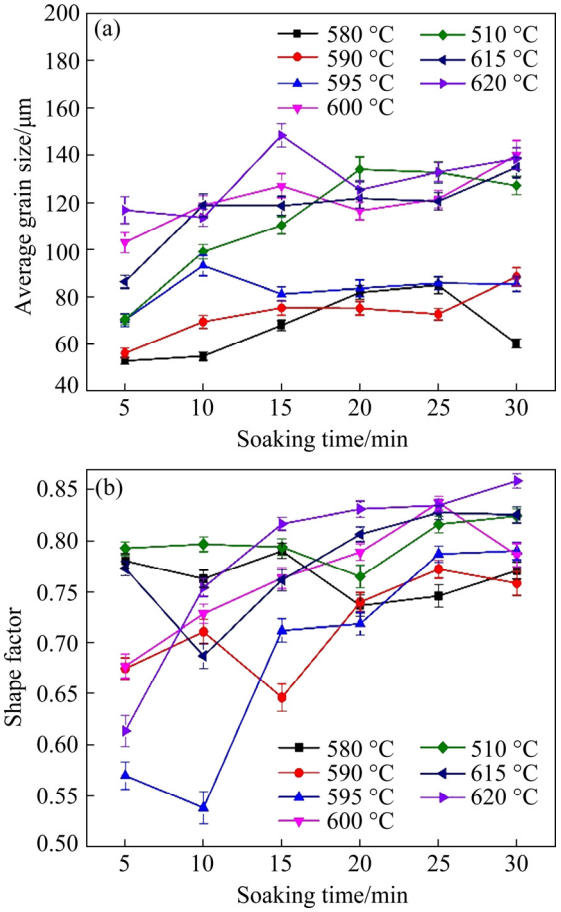

Fig. 12 Average grain size (a) and shape factor (b) on ND surface of 2A14 aluminum alloy after isothermal treatment at different temperatures for different soaking time

the extension of the holding time [43,47,48]. This may indicate that the average size of solid particles has a limit size during the isothermal process in the semi-solid temperature range. Because in this study, the size of the solid phase particles increases slowly with the extension of the holding time, then becomes stable and even occasionally decreases (at 620 °C for 15−20 min, at 595 °C for 10−15 min, at 600 °C for 15−20 min) with the extension of the holding time. And the size of the solid particles in this study is much larger than other studies [48].

The coarsening kinetics of semi-solid solid particles is usually fitted by the LSW empirical formula [35,36]. There is a linear relationship between the cube of solid-phase particle diameter and time, as

$$D_t^n - D_0^n = Kt \tag{4}$$

where D_t is the average grain diameter at the holding time t, D_0 is the initial average grain

diameter, K is the coarsening rate constant, and n is the coarsening exponent.

As shown in Fig. 13 and Table 3, attempts to fit the cube of the grain diameter with the formula failed to meet the LSW coarsening kinetics. The closer the linear correlation coefficient (R^2) to 1, the stronger the linear correlation, and the closer the R^2 to 0, the weaker the linear relationship. When the R^2 is less than 0, the linear relationship is absence. At 580, 590, 610 and 615 °C, the fitting coarsening slopes (K) were 360, 114, 1130 and 993, respectively. At 595 °C, the fitting coarsening slope K was 3.75, close to 0. At 600 and 620 °C, the fitting coarsening slope K was −340 and −401, respectively. The R^2 at all temperatures was low, and the R^2 was even negative at 590, 595, 600 and 620 °C. For this result, two aspects of information can be summarized. On the one hand, the coarsening behavior of grain size with the extension of isothermal time was not obvious. The evolution behavior of solid particles in the isothermal process was more complicated, and the result of the superposition of coarsening and melting phases was uncertain. On the other hand, the evolution of grain size over time cannot be described by the classic LSW empirical formula. This may be due to the lack of deformation and energy storage in the hot-rolled structure, and the solid grain size of the structure obtained by recrystallization at the early stage of heating was relatively coarse, so that the coarsening behavior was not obvious when the isothermal time was extended in the later stage.

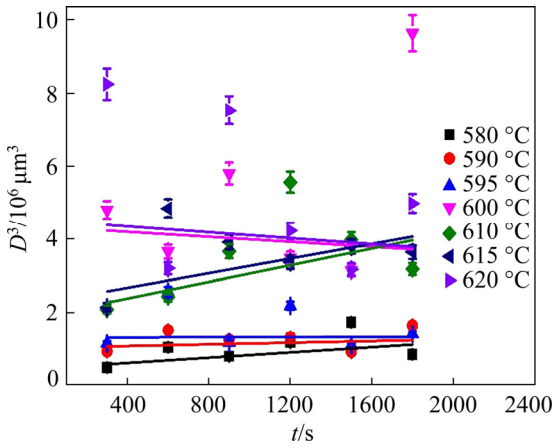

Fig. 13 Coarsening rate constant of 2A14 aluminum alloys after isothermal treatment under different conditions

Table 3 Linear fit results of D^3–t scatter plot

Temperature/°C	Slope	R^2
580	360	0.287
590	114	−0.184
595	3.75	−0.250
600	−340	−0.233
610	1130	0.338
615	993	0.255
620	−401	0.228

In addition, the fact that the grain growth mechanism is dominated by coalescence is also a reason why LSW is not applicable. The method used in this work is to directly heat elongated grains to the semi-solid state for isothermal holding, while the orientations of elongated grains are similar. The microstructure evolution in the manuscript showed that the coarsening mechanism is dominated by coalescence. JIANG et al [33] pointed out that LSW coarsening kinetics is suitable to describe the growth dominated by Ostwald ripening mechanism. This also verifies the grain coarsening mechanism, and the coarsening mechanism is dominated by coalescence.

4 Conclusions

(1) The optimum conditions are holding at 615 °C for 20 min, corresponding to the solid phase fraction of 0.61, which has an average grain size of 124 μm and a shape factor of 0.81 on the ND surface.

(2) Complete recrystallization occurs when the sample is heated to 600 °C. Increasing the temperature can promote the recrystallization process to obtain a more uniform solid−liquid phase distribution. The solid particle size on the ND surface is uniform and the roundness is good. The solid phase particles on the RD surface are not uniform in size and irregular in shape. On the TD surface, the solid phase is composed of a small number of equiaxed grains and most elongated grains.

(3) Coarsening of the solid particles occurred before holding time of 15 min, and grain size was stable after 15 min. The coarsening mechanism is dominated by coalescence, and the Ostwald ripening mechanism is not obvious. The LSW coarsening kinetics is not suitable for describing the change law of grain size during the isothermal process.

(4) Distribution of elements is similar to the distribution of solid−liquid phases. The solid phase is an aluminum solid solution with a small amount of alloying elements dissolved. The alloying elements are mainly distributed in the liquid phase and exist as eutectic components with low melting points.

Acknowledgments

This work was financially supported by the National Natural Science Foundation of China (No. 51875124), and the National Key Research and Development Project, China (No. 2019YFB2006503).

References

[1] HUANG L P, HE L L, CHEN S Y, CHEN K H, LI J Y, LI S, LIU W S. Effects of non-isothermal aging on microstructure, mechanical properties and corrosion resistance of 2A14 aluminum alloy [J]. Journal of Alloys and Compounds, 2020, 842: 155542.

[2] MA L, ZHOU C Z, SHI Y, CUI Q H, JI S D, YANG K. Grain- refinement and mechanical properties optimisation of A356 casting Al by ultrasonic-assisted friction stir processing [J]. Metals and Materials International, 2021, 27(2): 5374−5388.

[3] WANG M, HUANG L P, LIU W S, MA Y Z, HUANG B Y. Influence of cumulative strain on microstructure and mechanical properties of multi-directional forged 2A14 aluminum alloy [J]. Materials Science and Engineering A, 2016, 674: 40−51.

[4] MAO X C, YI Y P, HUANG S Q, GUO W F, HE H L, QUE J R. Effects of warm saddle forging deformation on the reduction of second-phase particles and control of the three-dimensional mechanical properties of 2219 aluminum alloy rings [J]. Materials Science and Engineering A, 2021, 804: 140737.

[5] WANG J, ZHOU D S, XIE L, LI X C, LU Y L, BAI Z H, ZHOU J H. Effect of multi-pass friction stir processing on microstructures and mechanical behaviors of as-cast 2A14 aluminum alloy [J]. Journal of Materials Engineering and Performance, 2021, 30: 3033−3043.

[6] LAN J, SHEN X J, LIU J, HUA L. Strengthening mechanisms of 2A14 aluminum alloy with cold deformation prior to artificial aging [J]. Materials Science and Engineering A, 2019, 745: 517−535.

[7] WANG Yong-fei, ZHAO Sheng-dun, ZHANG Chen-yang. Microstructures and mechanical properties of semi-solid squeeze casting ZL104 connecting rod [J]. Transactions of Nonferrous Metals Society of China, 2018, 28: 235−243.

[8] CHENG Shu-jian, ZHAO Yu-hong, HOU Hua, JIN Yu-chun, GUO Xiao-xiao. Preparation of semi-solid ZL101 aluminum alloy slurry by serpentine channel [J]. Transactions of Nonferrous Metals Society of China, 2016, 26: 1820−1825.

[9] CHEN Gang, ZHANG Yu-min, DU Zhi-ming. Mechanical behavior of Al−Zn−Mg−Cu alloy under tension in semi-solid state [J]. Transactions of Nonferrous Metals Society of China, 2016, 26: 643−648.

[10] JIANG J F, LIU Y Z, XIAO G F, WANG Y, XIAO X Q. Effects of plastic deformation of solid phase on mechanical properties and microstructure of wrought 5A06 aluminum alloy in directly semisolid thixoforging [J]. Journal of Alloys and Compounds, 2020, 831: 154748.

[11] SAMAT S, OMAR M Z, BAGHDADI A H, MOHAMED I F, AZIZ A M. Mechanical properties and microstructures of a modified Al−Si−Cu alloy prepared by thixoforming process for automotive connecting rods [J]. Journal of Materials Research and Technology, 2021, 10: 1086−1102.

[12] CHEN Q, CHEN G, JI X H, HAN F, ZHAO Z D, WAN J, XIAO X Q. Compound forming of 7075 aluminum alloy based on functional integration of plastic deformation and thixoformation [J]. Journal of Materials Processing Technology, 2017, 246: 167−175.

[13] ABBASIPOUR B, NIROUMAND B, MONIR VAGHEFI S M, ABEDI M. Tribological behavior of A356−CNT nanocomposites fabricated by various casting techniques [J]. Transactions of Nonferrous Metals Society of China, 2019, 29: 1993−2004.

[14] FLEMINGS M C. Behavior of metal alloys in the semisolid state [J]. Metallurgical Transactions A, 1991, 22: 957−981.

[15] CHEN C P, TSAO C Y A. Semi-solid deformation of non-dendritic structures—I. Phenomenological behavior [J]. Acta Materialia, 1997, 45: 1955−1968.

[16] SPENCER D B, MEHRABIAN R, FLEMINGS M C. Rheological behavior of Sn−15 pct Pb in the crystallization range [J]. Metallurgical and Materials Transactions B, 1972, 3: 1925−1932.

[17] BUSTOS O, LEIVA R, SÁNCHEZ C, ORDOÑEZ S, CARVAJAL L, MANNHEIM R. Microstructural evolution and rheological properties of AA6063 alloy produced by semisolid processing (SIMA and MHD) [J]. Revista De Metalurgia, 2007, 43: 165−180.

[18] GULER K A, KISASOZ A, OZER G, KARAASLAN A. Cooling slope casting of AA7075 alloy combined with reheating and thixoforging [J]. Transactions of Nonferrous Metals Society of China, 2019, 29: 2237−2244.

[19] YOUNG K P, KYONKA C P, COURTOIS J A. Fine grained metal composition: US4415374 [P]. 1983−11−15.

[20] KIRKWOOD D H, SELLARS C M, ELIASBOYED L G. Thixotropic materials: US5037489 [P]. 1991−08−06.

[21] JIANG J F, WANG Y, XIAO G F, NIE X. Comparison of microstructural evolution of 7075 aluminum alloy fabricated by SIMA and RAP [J]. Journal of Materials Processing Technology, 2016, 238: 361−372.

[22] CAMPO K N, LOPES E S N, PARRISH C J, CARAM R. Rapid quenching of semisolid Ti−Cu alloys: Insights into globular microstructure formation and coarsening [J]. Acta Materialia, 2017, 139: 86−95.

[23] CZERWINSKI F. Thermomechanical processing of metal feedstock for semisolid forming: A review [J]. Metallurgical and Materials Transactions B, 2018, 49: 3220−3257.

[24] LI K N, ZHANG Y B, ZENG Q, HUANG G H, JI B, YIN D D. Effects of semisolid treatment and ECAP on the microstructure and mechanical properties of

Mg−6.52Zn−0.95Y alloy with icosahedral phase [J]. Materials Science and Engineering A, 2019, 751: 283−291.
[25] MESHKABADI R, FARAJI G, JAVDANI A, POUYAFAR V. Combined effects of ECAP and subsequent heating parameters on semi-solid microstructure of 7075 aluminum alloy [J]. Transactions of Nonferrous Metals Society of China, 2016, 26: 3091−3101.
[26] BINESH B, AGHAIE-KHAFRI M. RUE-based semi-solid processing: Microstructure evolution and effective parameters [J]. Materials & Design, 2016, 95: 268−286.
[27] TAO J Q, JIANG J F, CHEN H, XIAO Y L, ZHANG R C, HU Q H, ZHAO J, ZHAO Q. Application of cyclic upsetting-extrusion to semi-solid processing of AZ91D magnesium alloy [J]. Transactions of Nonferrous Metals Society of China, 2013, 23: 909−915.
[28] CAO M, ZHANG Q, ZHANG Y S. Effects of plastic energy on thixotropic microstructure of C5191 alloys during SIMA process [J]. Journal of Alloys and Compounds, 2017, 721: 220−228.
[29] HAGHDADI N, ZAREI-HANZAKI A, HESHMATI-MANESH S, ABEDI H R, HASSAS-IRANI S B. The semisolid microstructural evolution of a severely deformed A356 aluminum alloy [J]. Materials & Design, 2013, 49: 878−887.
[30] XIAO G F, JIANG J F, LIU Y Z, WANG Y, GUO B Y. Recrystallization and microstructure evolution of hot extruded 7075 aluminum alloy during semi-solid isothermal treatment [J]. Materials Characterization, 2019, 156: 109874.
[31] POLA A, TOCCI M, KAPRANOS P. Microstructure and properties of semi-solid aluminum alloys: A literature review [J]. Metals, 2018, 8: 181.
[32] CHEN G, CHEN Q, QIN J, DU Z M. Effect of compound loading on microstructures and mechanical properties of 7075 aluminum alloy after severe thixoformation [J]. Journal of Materials Processing Technology, 2016, 229: 467−474.
[33] JIANG J F, LIU Y Z, XIAO G F, WANG Y, XIAO X Q. Effects of temperature and time on microstructural evolution of semisolid 5A06 aluminum alloy: Preparation of semisolid billets in ellipsoid solid phase [J]. Journal of Materials Engineering and Performance, 2020, 29: 5346−5359.
[34] JIANG J F, XIAO G F, WANG Y, QI Y S. Microstructure evolution of wrought nickel based superalloy GH4037 in the semi- solid state [J]. Materials Characterization, 2018, 141: 229−237.
[35] LIFSHITZ I M, SLYOZOV V V. The kinetics of precipitation from supersaturated solid solutions [J]. Journal of Physics and Chemistry of Solids, 1961, 19: 35−50.
[36] WAGNER C. Theory of the ageing of precipitates by redissolution (Ostwald maturing) (in German) [J]. Electrochemistry, 1961: 581−591.
[37] ZHANG D Y, DONG H B, ATKINSON H. What is the process window for semi-solid processing? [J]. Metallurgical and Materials Transactions A, 2016, 47: 1−5.
[38] FIELD D P, BRADFORD L T, NOWELL M M, LILLO T M. The role of annealing twins during recrystallization of Cu [J]. Acta Materialia, 2007, 55: 4233−4241.
[39] GHAZANLOU S I, EGHBALI B, PETROV R. Microstructural evolution and strengthening mechanisms in Al7075/ graphene nano-plates/ carbon nano-tubes composite processed through accumulative roll bonding [J]. Materials Science and Engineering A, 2021, 807: 140877.
[40] JO M C, JO M C, ZARGARAN A, SOHN S S, KIM N J, LEE S. Effects of Al addition on tensile properties of partially recrystallized austenitic TRIP/TWIP steels [J]. Materials Science and Engineering A, 2021, 806: 140823.
[41] WANG Y F, ZHAO S D, ZHAO X Z, ZHAO Y Q. Microstructural coarsening of 6061 aluminum alloy semi-solid billets prepared via recrystallization and partial melting [J]. Journal of Mechanical Science and Technology, 2017, 31: 3917−3923.
[42] ATKINSON H V, BURKE K, VANEETVELD G. Recrystallisation in the semi-solid state in 7075 aluminium alloy [J]. Materials Science and Engineering A, 2008, 490: 266−276.
[43] TZIMAS E, ZAVALIANGOS A. Evolution of near-equiaxed microstructure in the semisolid state [J]. Materials Science and Engineering A, 2000, 289: 228−240.
[44] YUN P W, ZHOU H H, FU H D, ZHANG Z H. A novel method to study recrystallization behavior: Continuous heating stress relaxation [J]. Materials Characterization, 2020, 167: 110500.
[45] WANG Y F, ZHAO S D, ZHANG C Y. Microstructural evolution of semisolid 6063 aluminum alloy prepared by recrystallization and partial melting process [J]. Journal of Materials Engineering and Performance, 2017, 26: 4354−4363.
[46] FU J L, WANG S X, WANG K K. Influencing factors of the coarsening behaviors for 7075 aluminum alloy in the semi-solid state [J]. Journal of Materials Science, 2018, 53: 9790−9805.
[47] JIANG J F, LIN X, WANG Y, QU J J, LUO S J. Microstructural evolution of AZ61 magnesium alloy predeformed by ECAE during semisolid isothermal treatment [J]. Transactions of the Nonferrous Metals Society of China, 2012, 22: 555−563.
[48] ATKINSON H V, LIU D. Coarsening rate of microstructure in semi-solid aluminium alloys [J]. Transactions of Nonferrous Metals Society of China, 2010, 20: 1672−1676.

温度和时间对半固态 2A14 铝合金短流程制备半固态坯三维组织演变的影响

刘英泽[1]，姜巨福[1]，肖冠菲[1]，张 颖[1]，黄敏杰[1]，王 迎[2]

1. 哈尔滨工业大学 材料科学与工程学院，哈尔滨 150001；
2. 哈尔滨工业大学 机电工程学院，哈尔滨 150001

摘 要：为了开发一种制备半固态坯料的短流程工艺，采用变形铝直接半固态等温处理(WADSSIT)工艺制备 2A14 铝合金半固态坯料。分析横截面、轧面、法面的三维组织演变。研究温度和保温时间对平均晶粒尺寸和平均形状因子的影响。结果表明，该工艺制备 2A14 半固态坯料的最佳条件为：在 615 ℃下保温 20 min，平均晶粒尺寸为 124 μm，形状因子为 0.81。电子背散射衍射(EBSD)观察表明，当加热到 600 ℃时，显微组织完全再结晶。晶粒尺寸随温度的升高而增大，随保温时间的延长而缓慢长大。圆度随保温时间的增加而增加，但对温度不敏感。

关键词：2A14 铝合金；三维显微组织；半固态坯料；组织演变

(Edited by Xiang-qun LI)